

Chapter 5

Control Strategy and Impact of Meshed DC Micro-grid in the Middle East



Mohamed Barara, Hervé Morel, Guy Clerc, Mustapha Jamma, Pascal Bevilacqua, and Abderrahime Zaoui

Abstract Installation of micro-grid provides as viable solution to the problem of energy efficiency and environmental in the world; this is especially true for countries in the Middle East which have an abundance of natural sunlight. Recently, DC micro-grids have been a focus of numerous researches, and some industrial deployments are starting (Shenai et al. *IEEE Power Electron. Mag.* 3:42–48, 2016). The interest is due to several advantages in comparison to AC micro-grids in terms of efficiency, minimum number of devices, no need for frequency/phase control, modularity, and reliability. Moreover, it enables an easy integration of renewable energy resources, particularly photovoltaic ones. This study targets meshed DC micro-grid while most of literature papers concern radial DC micro-grids. It will bring several remarkable benefits: redundancy, better utilization of installed converters, flexible configuration, enhanced system reliability, and availability especially in case of line faults (Chen et al. *IEEE Trans. Power Deliv.* 31:1719-1727, 2016). In meshed DC grids, the control strategy of current or power becomes a critical issue particularly if a modular and generic solution is researched. The study focuses on the use of smart nodes controlling the power flow in the grid. The proposed control strategy is modeled and the simulation results are presented. A reduce scale tests based on DSPACE DS1103 have been provided to validate experimentally the proposed control scheme.

Keywords DC Micro-grids · Smart nodes · Renewable energy sources · Middle East · split-PI converter · DSPACE DS1103

M. Barara (✉)

IBISC, University Evry, Université Paris-Saclay, Evry, France

H. Morel · P. Bevilacqua · A. Zaoui

University Lyon, INSA Lyon, CNRS, Ampère, Lyon, France

G. Clerc

University Lyon, Lyon 1, Ampère, Lyon, France

M. Jamma

Mohammed V University, Mohammadia School of Engineers, Rabat, Morocco

© Springer Nature Switzerland AG 2019

H. Qudrat-Ullah, A. A. Kayal (eds.), *Climate Change and Energy Dynamics in the Middle East*, Understanding Complex Systems, https://doi.org/10.1007/978-3-030-11202-8_5

109

1 Introduction

Natural energy flows (sun or heat,...) represent a large potential of renewable energy sources in the Middle East, in particular solar power. According to report by the electrical department at King Saud University, the Middle East receives 3000–3500 hours of sunshine per year, with more 5 KW/m of solar energy per day that are expected to play a considerable role of source of DC micro-grid.

Micro-grids are defined as small-scale grids that generate and deliver electricity to a defined geographic area, such as a building, a district, or an isolated location. They can be operated in islanded or grid-connected mode. Micro-grid architectures can be classified into AC or DC bus interconnections, as shown in Fig. 5.1, that is a kind of power grid area which is a combination of different kinds of power units which are usually based on renewable energy sources (Lu et al. 2011).

In an AC micro-grid, synchronization of all AC generators and output of the power converters of the DC sources and energy stores is necessary. Furthermore, due to the nonlinear characteristics of power electronics converters, power factor correction and topologies with sophisticated control strategy for harmonic distortion reduction are needed to improve the power quality of the AC bus (Oday 2011). The DC micro-grids have advantages over conventional AC micro-grids in the utilization of green power sources, since they can interface with DC systems more easily than AC systems, using simple power electronics. DC micro-grids present various advantages such as a better efficiency, no need for frequency/phase control, and higher reliability (Rey-López et al. 2015). Moreover most of the modern loads like computers, LED lighting, and electric vehicles work on DC power.

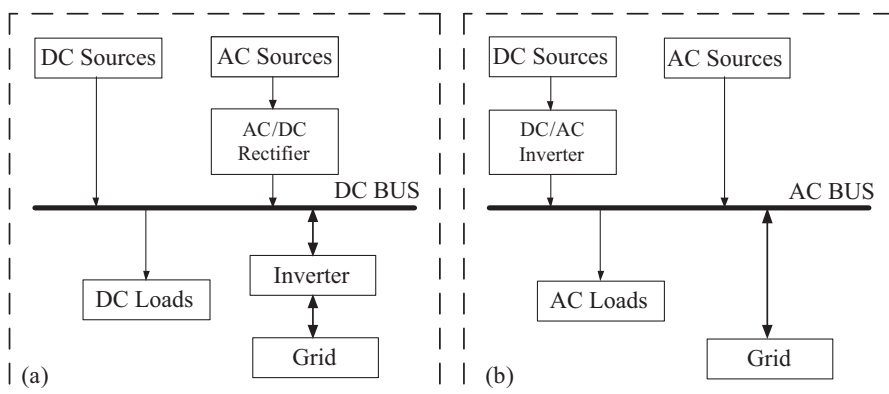


Fig. 5.1 Micro-grid topology. (a) Basic structure of DC micro-grid, (b) basic structure of AC micro-grid

1.1 DC Micro-grid System Configuration

A home power system can be divided into three parts: sources, distribution, and loads. Various power converters are usually required to adjust generator and load voltages to the DC bus voltage.

The radial structure of DC micro-grid is shown in Fig. 5.2. Renewable energy module is firstly used to provide the energy to the grid for the energy storage module or for the load module (Liu et al. 2010). Then, if the demand energy is not enough from the renewable energy module, the AC power supply will distribute the energy to the DC micro-grid by the bidirectional AC/DC converter. In addition, if the AC power supply is absent due to any unexpected case, the DC diesel generation system will serve as the standby energy module to offer the energy for the grid. Finally, the DC power will flow to the output load module, which includes three types of loads.

1.2 Standards and Research

Global architecture standards required for widespread implementation of 400 V DC are well under way. Micro-grids are being studied by a number of instances, as part of the smart grid research programs. DC micro-grids are an emerging option as a result of these programs. Examples of such emerging standards are (Rycroft 2014):

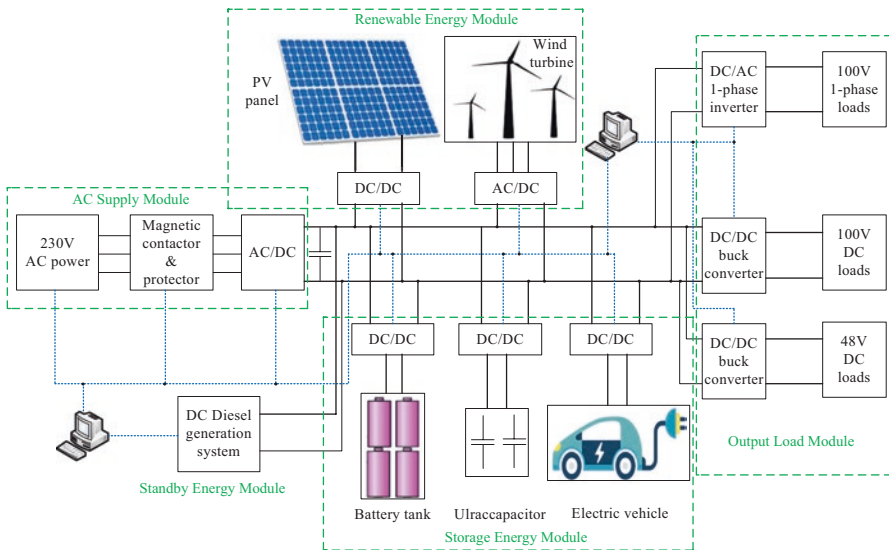


Fig. 5.2 Radial structure of DC micro-grid

- Emerge Alliance: An industry association in conjunction with the EPRI task force is working on a 380 V DC standard to cover telecom and building distribution.
- The European Telecommunications Standards Institute (ETSI) standard: 400 V DC distribution for telecommunications equipment, (ETSI) EN 300132-3-1, released in February 2012. This is primarily intended for use in the telecommunications industry but contains several useful sections which can be transferred to other sectors.
- IEC: SG4 is working on a standard for LVDC distribution with a nominal voltage of 400 V but covering systems up to 1500 V.

Distribution generators in DC micro-grid are connected to a common DC bus using power electronic converters; the common DC voltage must be well maintained with a limited variation band. Ferreira et al. 2012 present a performance study of a DC micro-grid when it is used as a voltage-droop technique to regulate the grid voltage and to control the load sharing between different sources. The control strategies presented in Jin et al. (2014) and Guerrero et al. (2011) consist of a hierarchical control strategy based of three levels of control: Primary control to ensure proper load sharing among the distributed generators, secondary control level to regulate the voltage deviations, and tertiary control level regulate the flow of power between the grid and micro-grid (Liu et al. 2010). So far, various studies have been carried out on radial micro-grid, while very limited research has been done in meshed DC micro-grid. However, it will bring several remarkable benefits: redundancy, better utilization of installed converters, flexible configuration, enhanced system reliability, and availability especially in case of line faults (Chen et al. 2016). Another advantage of meshed DC micro-grid is the ability to reduce the total wire length by minimizing the distance between a load and a grid node, particularly for high power line, that may reduce the global cost of the grid and reduce the needed mass of copper for the same operation.

In meshed DC grids, the control strategy of current or power becomes a critical issue particularly if a modular and generic solution is researched. There are several control strategies for meshed MTDC grids that have been investigated in the literature and will be helpful for the application of meshed DC micro-grid. In a point-to-point link, one converter controls the voltage of the line, and the other one controls the current by a method like the voltage margin method (Nakajima and Irokawa 1999). In a multiterminal DC grid, it is very important to control the power flow by control-flow converters like split-PI converters. A DC current flow controller for meshed modular multilevel converter multiterminal HVDC grids has been designed and demonstrated in Deng et al. (2015). Chen et al. (2016) proposed a novel interline DC power flow controller for meshed HVDC Grids for achieving stable power flow control in different conditions. In Yao et al. (2016), the authors present a DC power flow controller based on dual active bridge (DAB) topology and its control strategy in the DC grid is also presented. Concretely, in this study, a topology of meshed DC micro-grid with a suitable and efficiency control scheme of bidirectional DC/DC converter is presented. The proposed control strategy plays an essential role to control the power flow in DC meshed micro-grid.

2 Targeted Mock-up

In the framework of the ANR project C3 μ and the GD3E/CPER project, a mock-up with 20 kW DC/DC converters is under construction (Fig. 5.3). In this mock-up a 20 kW PV panel and a 20 kW electric vehicle plug-in will be emulated. The connection to the AC-grid will be emulated too. The mock-up includes two branches in order to analyze meshed DC micro-grid behavior. In practice, the two branches enable a power flow controlled by a smart node from the PV panel toward the EC plug-in. The system configuration of the targeted mock-up is depicted in Fig. 5.3. Our project deals with meshed DC micro-grids which have the benefit of a simple control, redundancy, and an automatic reconfiguration of the micro-grid (in case of faults or with extensions of the grid). The project focuses on the use of smart nodes to achieve flexible power flow control for the grid. Other tasks will be developed at the end of the project such as consumption measure, transmission, and data processing for exchange between the smart plug and the smart nodes and the centralized supervision even with a decentralized supervision system.

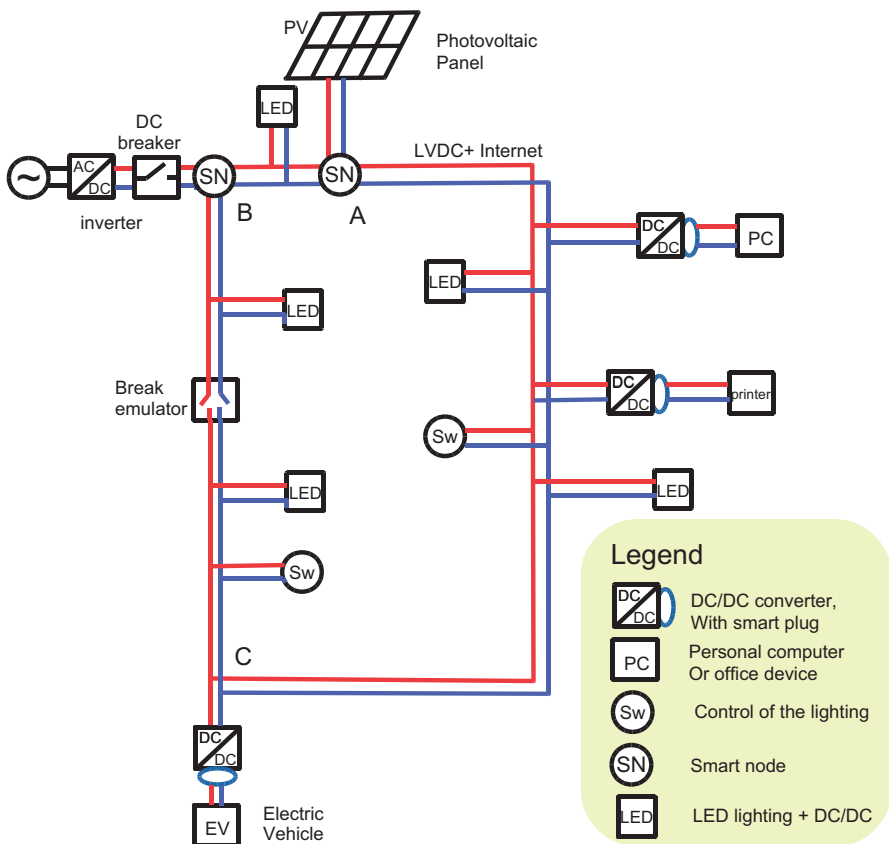


Fig. 5.3 Principle scheme of the targeted mock-up

3 Smart Node

A smart node consists of three power lines with two lines connected via a bidirectional DC/DC converter as shown in Fig. 5.4. Each converter is driven by a controller for generating PWM signals. A communication layer (as Ethernet) enables to communicate with decentralized supervision system for all required data such as the output voltages and currents. Another target of the project is to use carrier current technology on the power line to enable the communication layer. The main objective of a smart node is to control the power flow in the meshed micro-grid. Another role of the smart node is to operate as a DC breaker.

So, the protection strategy will be based on smart node with DC breaking capability. Consequently, each source in the grid must be connected to the meshed DC micro-grid via a smart node (Fig. 5.3). DC breaking capability is the target of an additional PhD study (Ma et al. 2017).

4 Proposed Control Strategy at a Converter Level

In a point-to-point link, one converter controls the voltage of the line, and the other one controls the current by a method like the voltage margin method (Ferreira et al. 2012). In a multiterminal DC grid, MTDC, the issue becomes further complex, and numerous papers proposed control scheme based on the droop control method (Ferreira et al. 2012; Haileselassie and Uhlen 2012; Hu and Weaver 2016). The latter case has some drawbacks as the use of virtual impedance, and our target is to apply a common control strategy to all the converters of the grid. The case of a meshed DC micro-grid is quite different because power flow converters are inserted in the lines to control the power flow, such as split-PI converters (Natori et al. 2014). However, in a general meshed DC grid, some converters must control the voltage,

Fig. 5.4 Smart node configuration

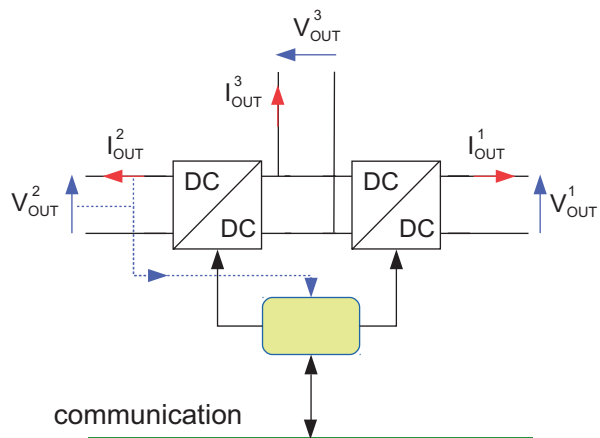
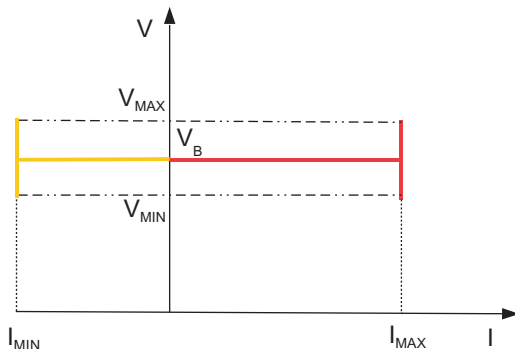


Fig. 5.5 Proposed steady-state control strategy for each output side of smart node converter. The controller may be set for a positive power (in red) or a negative power (in yellow)



and other ones control the line current. So, a straightforward question is: Which value of voltage has to be applied when the voltage is controlled?

Since a modular solution is targeted with no need of complex controller settings, our proposal is to apply the unique bus voltage in such a case. In our targeted mock-up, the reference bus voltage is selected to = 400 V. In the case where the line current has to be controlled, a steady-state strategy inspired from the voltage margin method is applied as shown in Fig. 5.5.

5 Bidirectional Buck-Boost Converter

Generally the bidirectional DC-DC converters are used in applications where bidirectional power flow may be necessary. The principal operation of this converter can be used to operate in both the buck and boost modes with bidirectional power control (Park et al. 2013). It could play a significant role in the future power management in DC meshed micro-grid. We focus in this study to control this type of power converter in order to realize power distribution between energy generation systems and loads systems. Number of topologies are proposed with different control strategies that have been reported in literature to transfer the power from one source to another (Phattanasak et al. 2011; Rathore et al. 2016). Bidirectional DC/DC converter can be classified into isolated and non-isolated; the non-isolated converter has more advantage of lower magnetic bulk, higher efficiency, and compactness.

5.1 Split-PI Converter

The split-PI converter topology (Fig. 5.6) allows bidirectional flow of power. In typical operation, the voltage is applied at the left-hand bridge and operates as a boost converter, and the right-hand bridge operates as a buck converter. When the

Fig. 5.6 Split-PI converter

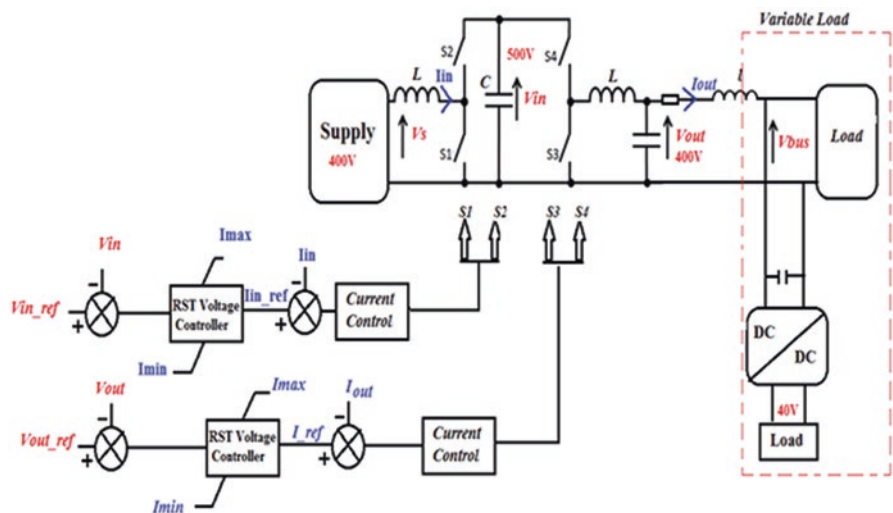
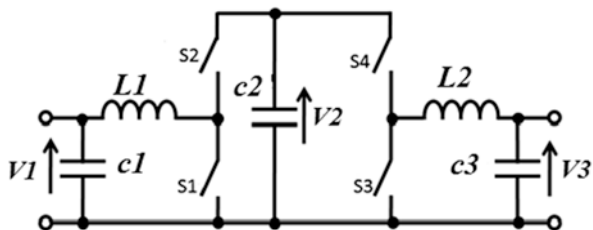


Fig. 5.7 Proposed control scheme for split-PI converter. Test configuration with a voltage source at the input and a variable load at the output

voltage is applied at the right-hand bridge, the reverse can be achieved (Singhai et al. 2014). The advantage of this converter is to reduce switching noise, since both ends of the converter are shielded by a capacitor and inductor resulting in triangular current wave forms, which contain fewer harmonics (Maclairin et al. 2011; Khan et al. 2014). And it is simpler to design, implement, and control.

5.2 Control Scheme for Split PI

Dual loop control layer is implemented to control current and voltage settings as shown in Fig. 5.7.

The control mechanism of the proposed bidirectional DC-DC converter is shown in Fig. 5.7. It consists of two separate RST voltage controllers in cascades with currents controllers, which are used to regulate the intermediate voltage (boost) and the output voltage (buck) with a maximal and minimal pre-defined current. This configuration can handle reference changes in both the intermediate stage and load side.

6 Results and Discussions

6.1 First Simulation Result

A practical control scheme has been defined as shown in Fig. 5.7. It has been tested in several configurations. The first one, presented in Fig. 5.7, corresponds to the case where the DC/DC converter is supplied by an ideal source in the input side and a variable load at the output side. This control has two operation modes: a voltage-mode control and current-mode control. Simulation results obtained using Matlab/Simulink are shown to validate the proposed controller performance. The parameters of the bidirectional DC-DC converter used in this study are listed in Table 5.1.

Load cases are used as described below:

Case A: $0 \text{ s} < t < 1 \text{ s}$

The load current is lower than I_{\max} ($I_{\text{out}} < I_{\max}$). The controller operates in a voltage-mode control, $V_{\text{out}} = V_{\text{bus}}$.

Case B: $1 \text{ s} < t < 2 \text{ s}$

The load current may be higher than I_{\max} ($I_{\text{out}} > I_{\max}$). The controller operates in a current-mode control, $I_{\text{out}} = I_{\max}$.

Case C: $2 \text{ s} < t < 3 \text{ s}$

The load current is lower than I_{\max} ($I_{\text{out}} < I_{\max}$). The controller returns to work as voltage-mode control, $V_{\text{out}} = V_{\text{bus}}$.

As observed in Figs. 5.8 and 5.9, the controller keeps the voltage at a fixed value of $V_{\text{out}} = V_{\text{bus}} = 400 \text{ V}$ (point A) because the output current is lower than the maximal current $I_{\max} = 45 \text{ A}$ as defined by the dispatching level. The observed oscillations are related to the high value of the line inductance of the targeted mock-up. After increasing the power of the load, the controller keeps the output current at fixed value of 45 A and the output voltage drop (point B). Finally, the control returns to voltage regulation, when the power of the load decreases and doesn't exceed I_{\max} (point C), while in all cases the intermediate voltage is always maintained at a constant value of 500 V .

Table 5.1 Specification of bidirectional DC/DC converter

Symbol	Parameter	Value
C	Capacitance	$3300 \mu\text{F}$
L	Inductance	$450 \mu\text{H}$
V	Voltage	500 V
A	Current	75 A

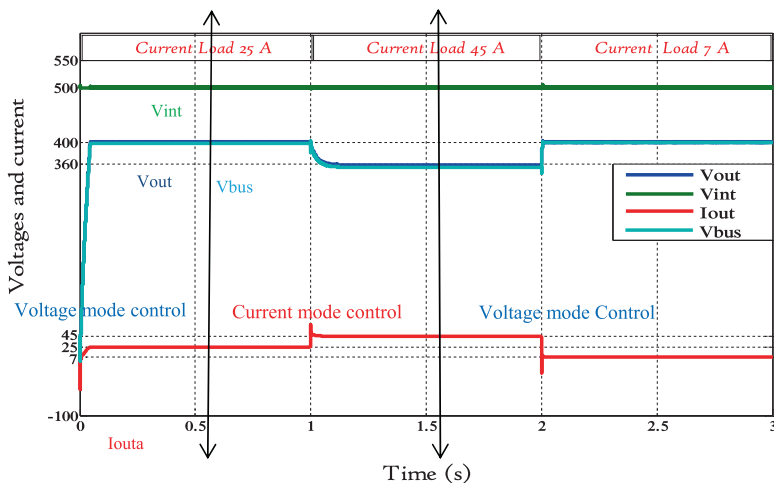


Fig. 5.8 Transient waveforms at sudden change in load (see Fig. 5.4), intermediate voltage, output voltage, output current, and DC bus voltage

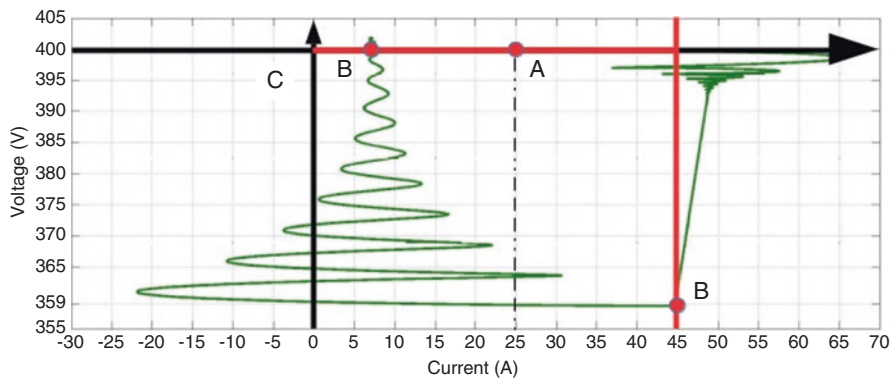


Fig. 5.9 Simulation results of voltage (V_{out}) and current (I_{out}) for different operation conditions

6.2 Experimental Results

A prototype split-PI converter has been built with a reduced power scale in order to validate our proposed control scheme. A DSPACE DS1103 is used to generate PWM states signals for the converter. The references voltages and limited currents are given by the control desk. The experimental setup is shown in Fig. 5.10. The system parameters used in simulation and experimentation are listed in Table 5.2.

Simulation and experiments are achieved with the same parameters. Figures 5.11, 5.12, 5.13, and 5.14 show the effect of a sudden variation of the load with limited current fixed at 0.7 A.

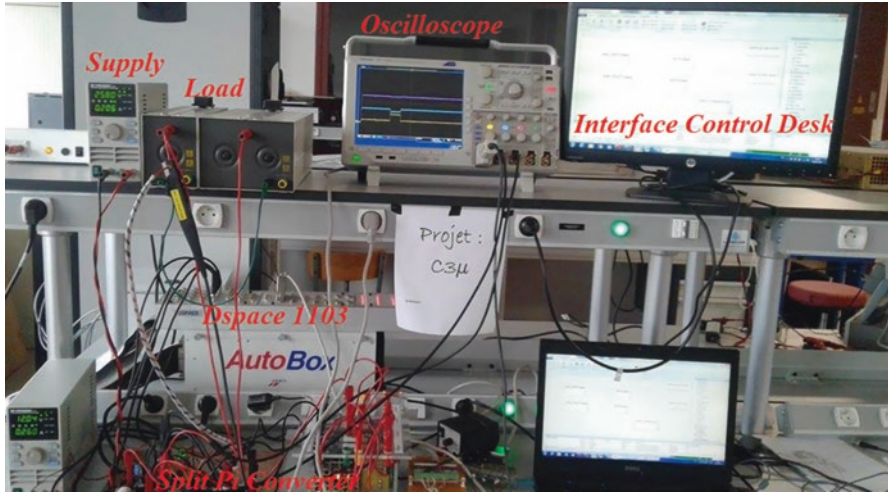


Fig. 5.10 Hardware used in experimental evaluation

Table 5.2 Simulation and experimental system parameters

Symbol	Parameter	Value
C	Capacitance	780 μ F
L	Inductance	2.2mF
R	Load	102.6 and 25.4 Ohm
A	Maximal current	0.75 A

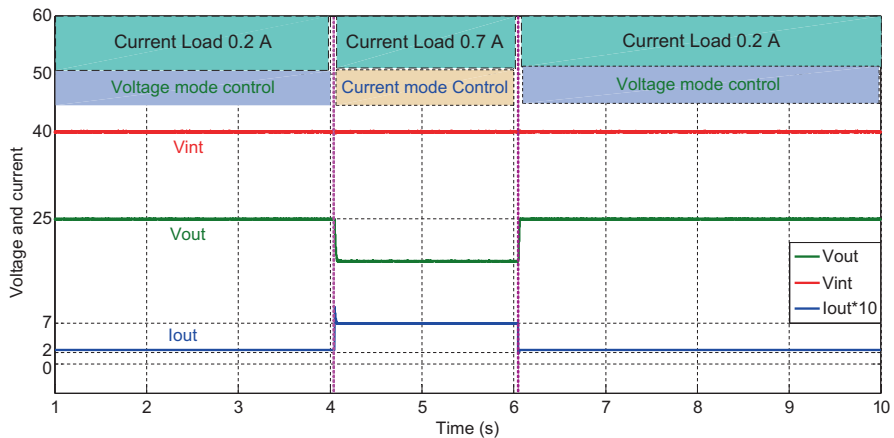


Fig. 5.11 Simulation results transient waveforms at sudden change in load, intermediate voltage (Vint), output voltage, and output current (Iout)

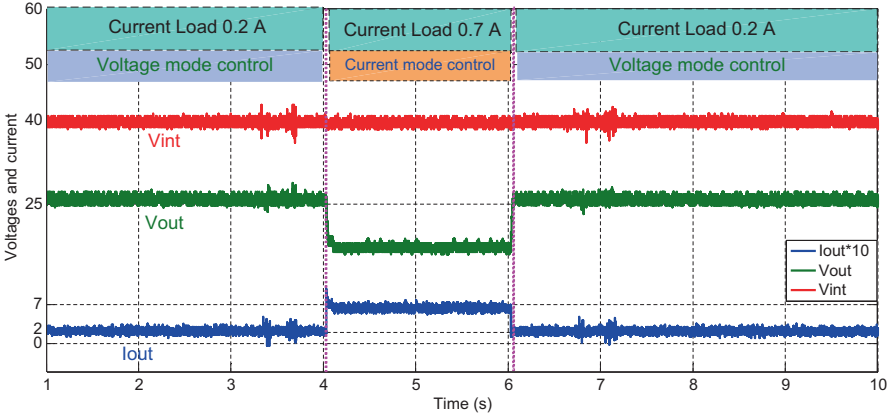


Fig. 5.12 Experimental results transient waveforms at a sudden change of load, intermediate voltage (Vint), output voltage, and output current (Iout)

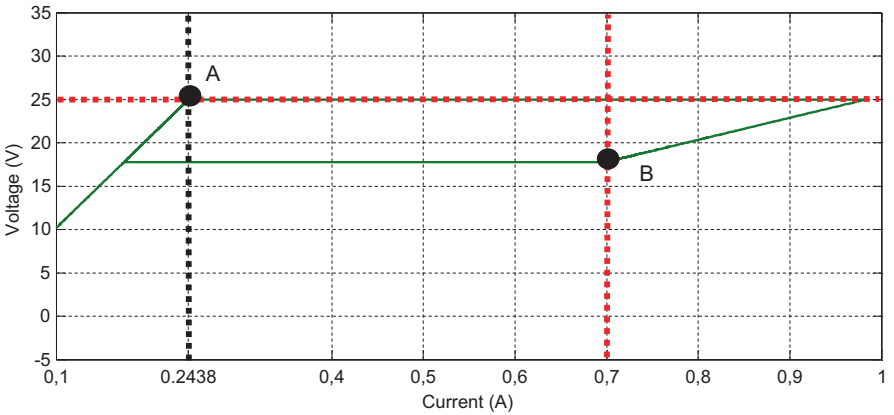


Fig. 5.13 Simulation results of voltage (Vout) and current (Iout) for different operations conditions

As it can be seen in Figs. 5.11 and 5.13, the measured results of the control present a good agreement with the simulation results in Figs. 5.12 and 5.14. It is observed that the output voltage (Vout) is regulated at a fixed value as given in reference ($V_{ref_out} = 25\text{ V}$), because output current is lower than the maximal current defined by the control desk ($I_{max} = 0.7\text{ A}$). After increasing the power of the load, the controller keeps the output current at a fixed value of 0.7 A and the output voltage drop. Finally, the control returns to voltage regulation when the load decreases and doesn't exceed I_{max} , while in all cases the intermediate voltage is always maintained at a constant value of 40 V. It can be easily found that the proposed control can achieve much higher efficiency.

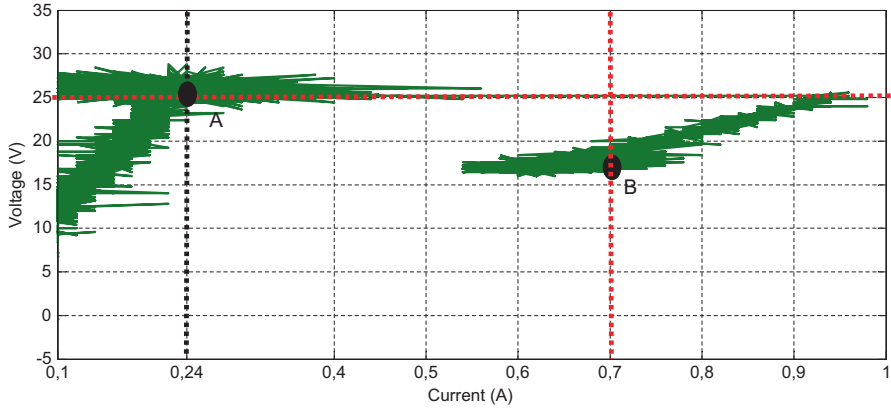


Fig. 5.14 Experimental results voltage (V_{out}) and current (I_{out}) for different operations conditions

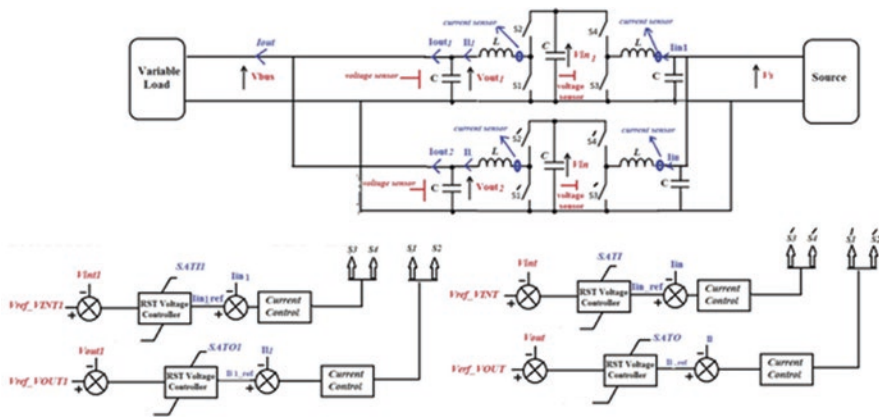


Fig. 5.15 Proposed control scheme for smart node

6.3 Experimental Results of Smart Node

A test configuration with a voltage source at the input and a variable load at the output is done in using the proposed control scheme for smart node as shown in Fig. 5.15.

A prototype of two split-pi converter has been built with a reduced power scale in order to validate our proposed control scheme. A DSPACE DS1103 is used to generate PWM states signals for the converters. The references voltages and limited currents are given by the control desk. The experimental test bench is shown in Fig. 5.16.

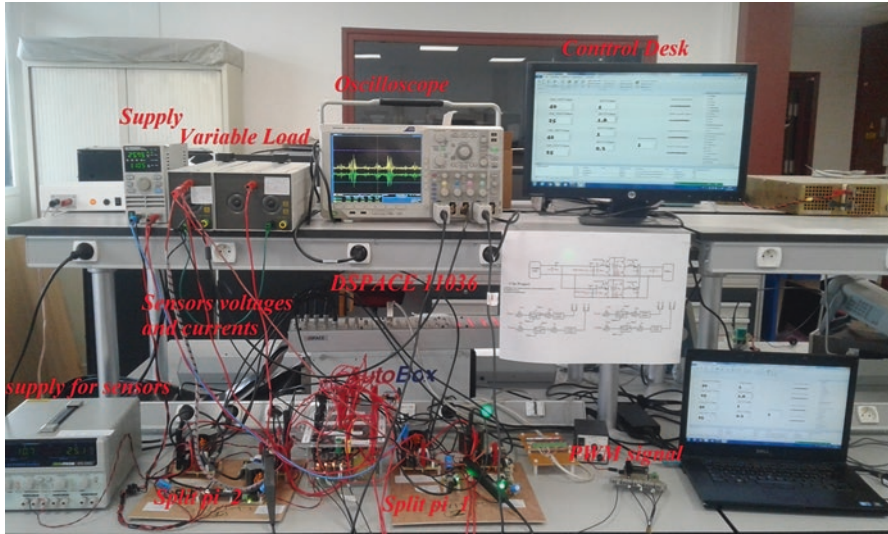


Fig. 5.16 Hardware used in experimental evaluation for smart node

Several test cases have been studied:

(a) Case 1

Converter 1 ensures regulation of DC bus voltage, and converter 2 ensures the regulation of current as depicted in Fig. 5.17:

- The total load current is 0.98 A.
- The reference output voltage for converter 1 and converter 2 is $V_{ref_out1} = v_{ref_out} = 25$ V.
- The reference intermediate voltage for converter 1 and converter 2 is $V_{ref_vint1} = v_{ref_vint} = 40$ V.
- The maximal currents of the converters are $i_{out1} = 0.4$ A and $i_{out2} = 0.8$ A (Fig. 5.18).

(b) Case 2

Converter 1 ensures regulation of current and converter 2 ensures the regulation of current:

- The total load current is 0.98 A.
- The reference output voltage for converter 1 and converter 2 is $V_{ref_out1} = v_{ref_out} = 25$ V.
- The reference intermediate voltage for converter 1 and converter 2 is $V_{ref_vint1} = v_{ref_vint} = 40$ V.
- The maximal currents of the converters are $i_{out1} = 0.4$ A and $i_{out2} = 0.4$ A (Fig. 5.19).

(c) Case 3

Converter 1 ensures regulation of current and converter 2 ensures the regulation of current:

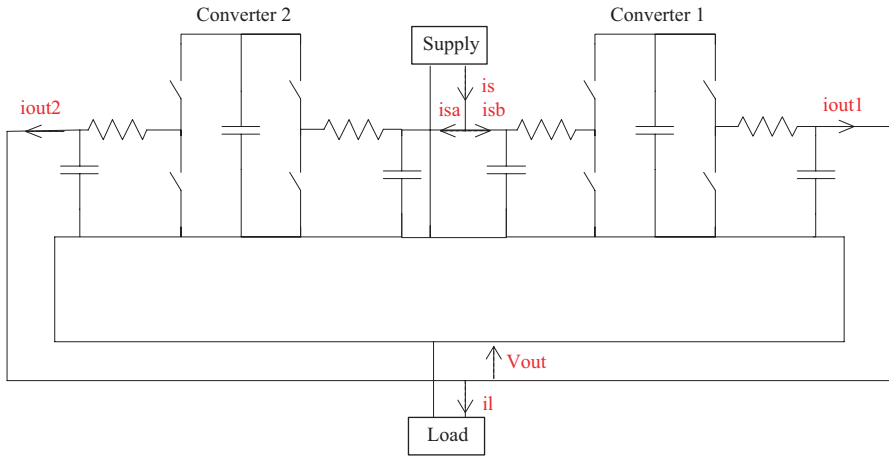


Fig. 5.17 System configuration of case 1, case 2, and case 3

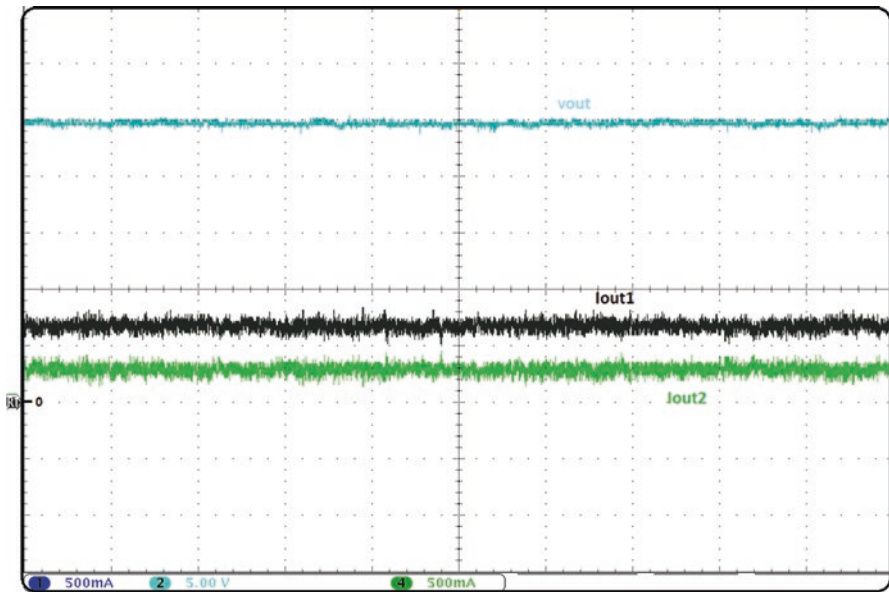


Fig. 5.18 Experimental results waveforms of output voltage (vout), output current of converter1 (iout1), and output current of converter2 (iout2)

- The total load current is 0.24A.
- The reference output voltage for converter 1 and converter 2 is $V_{ref_out1} = 25\text{ V}$ and $v_{ref_out} = 26\text{ V}$.
- The reference intermediate voltage for converter 1 and converter 2 is $V_{ref_vint1} = v_{ref_vint} = 40\text{ V}$.

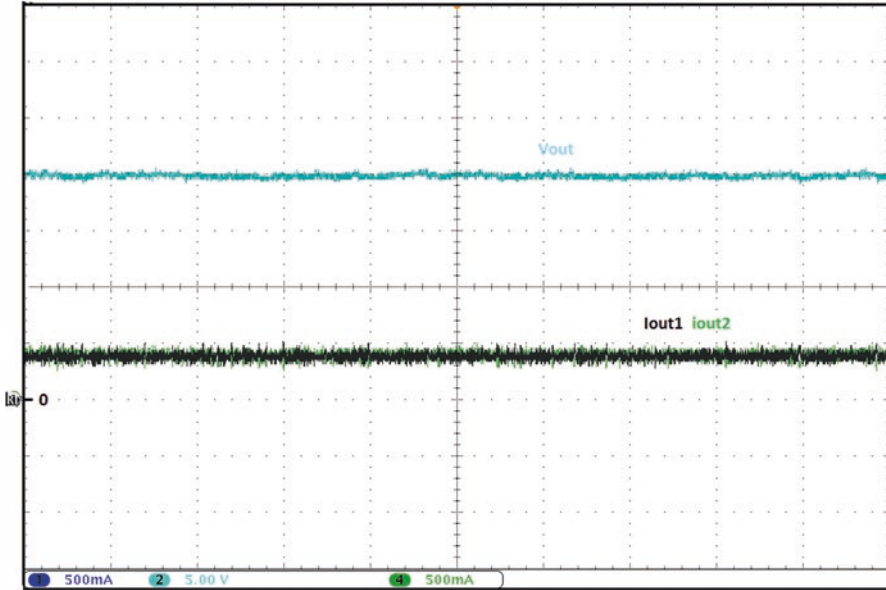


Fig. 5.19 Experimental results waveforms of output voltage (v_{out}), output current of converter1 (i_{out1}), and output current of converter2 (i_{out2})

- The maximal currents of the converters are $i_{out1} = 1$ A and $i_{out2} = 1$ (Fig. 5.20).

(d) Case 4

Converter 1 ensures regulation of current and converter 2 ensures the regulation of current as shown in Fig. 5.21:

The total load current is 0.24A.

The reference output voltage for converter 1 and converter 2 is $V_{ref_out1} = 26$ V and $v_{ref_out} = 25$ V.

The reference intermediate voltage for converter 1 and converter 2 is $V_{ref_vint1} = v_{ref_vint} = 40$ V.

The maximal currents of the converters are $i_{out1} = 0.4$ A and $i_{out2} = 1$ (Fig. 5.22).

As we can see from all cases of experiment test, the controller is well implemented for two bidirectional split-pi converters and effectively tracks to their reference value of voltage or current defined by the decentralized supervision system.

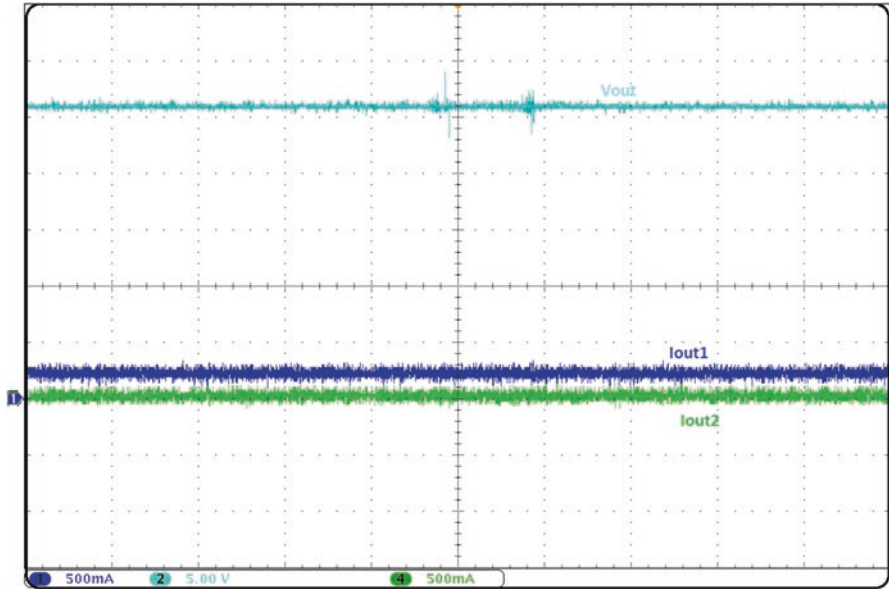


Fig. 5.20 Experimental results waveforms of output voltage (v_{out}), output current of converter1 (i_{out1}), and output current of converter2 (i_{out2})

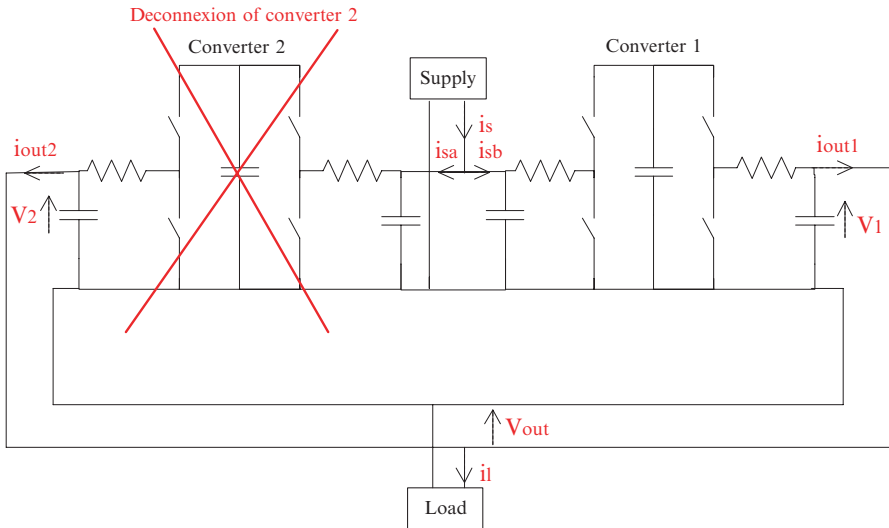


Fig. 5.21 System configuration of case 4

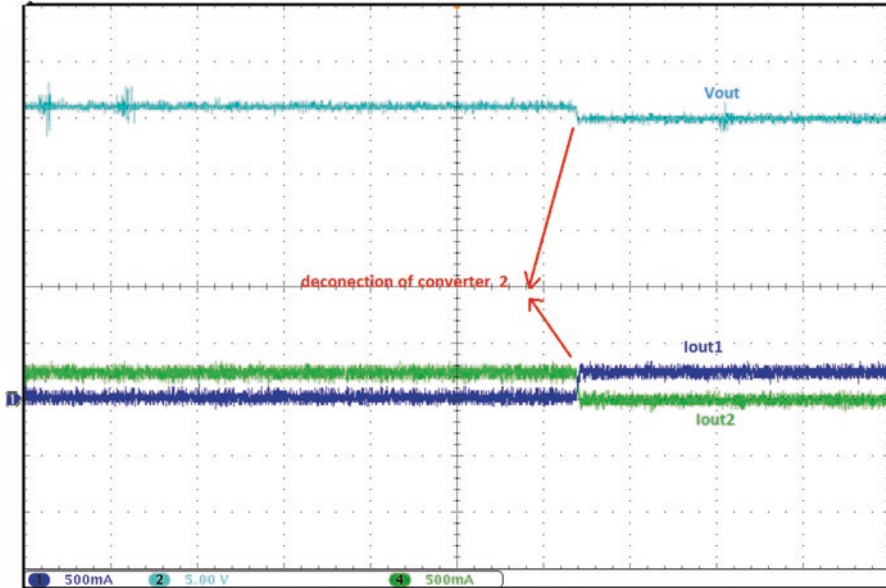


Fig. 5.22 Experimental results waveforms of output voltage (V_{out}), output current of converter1 (i_{out1}), and output current of converter2 (i_{out2})

7 Conclusion

The Middle East is in the early stages of smart grid development; this study contributes to renewable energy development in this region, by proposing a novel system operation strategy of DC meshed micro-grid with voltage and current-mode control for the power converter. The simulations test helps to visualize the response from the system and prove the certainty of the proposed algorithm. Experimental test of the power flow in the smart node with DSPACE DS1103 implementation with a reduced power scale using the combined controllers is also presented.

The next step of our work will be the improvement of the regulation of the voltage (V_2) between the two split-pi converters of the smart node (Fig. 5.23).

Today this function is realized by a compensating loop which uses the capacitor energy storage within acceptable operating limits in order to improve the voltage regulation of the central node.

In the future, we will try to realize a multi-output multi-input state robust regulation in order to take into account all the output and internal capacitor voltages. All these algorithms will be implemented in the 20 kW converters of our test bench (Fig. 5.24).

We will also increase the size and complexity of our DC network by emulating a photovoltaic injection and a charging terminal.

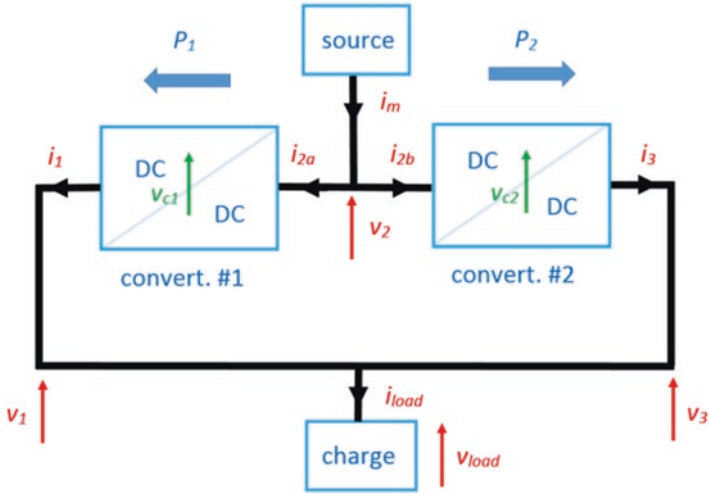
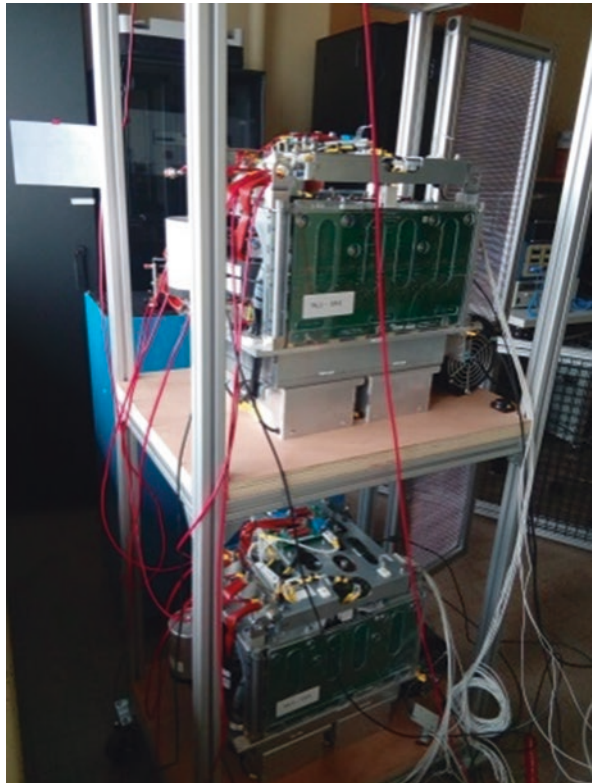


Fig. 5.23 Simplified DC network

Fig. 5.24 20 kW split PI



For the first test, a centralized supervision of the mock-up was applied based on Labview. In the future, we plan to develop a decentralized supervision of the DC meshed grid in the smart node which will be in charge of the energy consumption minimization and the high-level control, such as a user order to switch on LED lighting or some element start and stop.

Acknowledgments The authors would like to thank the ANR project C3 μ and the GD3E/CPER for the project funding.

References

- Chen, W., Zhu, X., Yao, L., Ning, G., Li, Y., Wang, Z., Gu, W., & Qu, X. (2016). A novel interline DC power-flow controller (IDCPF) for Meshed HVDC grids. *IEEE Transactions on Power Delivery*, *31*, 1719–1727.
- Deng, N., Wang, P., Zhang, X.-P., Tang, G., & Cao, J. (2015). A DC current flow controller for meshed modular multilevel converter multiterminal HVDC grids. *CSEE Journal of Power and Energy Systems*, *1*, 43–51.
- Ferreira, R. A. F., Braga, H. A. C., Ferreira, A. A., & Barbosa, P. G. (2012). *Analysis of voltage droop control method for dc microgrids with Simulink: Modelling and simulation*. In 2012 10th IEEE/IAS International Conference on Industry Applications. INDUSCON 2012, IEEE, Fortaleza, CE, Brazil, pp. 1–6.
- Guerrero, J. M., Vasquez, J. C., Matas, J., de Vicuna, L. G., & Castilla, M. (2011). Hierarchical control of droop-controlled AC and DC microgrids—A general approach toward standardization. *IEEE Transactions on Industrial Electronics*, *58*, 158–172.
- Haileselassie, T. M., & Uhlen, K. (2012). Impact of DC line voltage drops on power flow of MTDC using droop control. *IEEE Transactions on Power Apparatus and Systems*, *27*, 1441–1449.
- Hu, R., & Weaver, W. W. (2016). Dc microgrid droop control based on battery state of charge balancing. In 2016 IEEE Power and Energy Conference at Illinois (PECI), Urbana, IL, USA, pp. 1–8.
- Jin, C., Wang, P., Xiao, J., Tang, Y., & Choo, F. H. (2014). Implementation of hierarchical control in DC microgrids. *IEEE Transactions on Industrial Electronics*, *61*, 4032–4042.
- Khan, M. A., Husain, I., & Sozer, Y. (2014). A bidirectional DC–DC converter with overlapping input and output voltage ranges and vehicle to grid energy transfer capability. *IEEE Journal of Emerging and Selected Topics in Power Electronics*, *2*, 507–516.
- Liu, C., Chau, K. T., Diao, C., Zhong, J., Zhang, X., Gao, S., & Wu, D. (2010). *A new DC micro-grid system using renewable energy and electric vehicles for smart energy delivery*. In 2010 IEEE Vehicle Power and Propulsion Conference. Presented at the 2010 IEEE Vehicle Power and Propulsion Conference (VPPC), IEEE, Lille, France, pp. 1–6.
- Lu, X., Guerrero, J., Teodorescu, R., Kerekes, T., Sun, K., & Huang, L. (2011). *Control of parallel-connected bidirectional AC-DC converters in stationary frame for microgrid application*. In 2011 IEEE Energy Conversion Congress and Exposition. Presented at the 2011 IEEE Energy Conversion Congress and Exposition (ECCE), IEEE, Phoenix, AZ, USA, pp. 4153–4160.
- Ma, T. T. H., Yahoui, H., Boubkari, F. B., Morel, H., Vu, H. G., & Siauve, N. (2017). *Building a Matlab/Simulink model of SiC JFET for the investigation of solid state DC breaker*. Grenoble: CoSys-DC.
- Maclaurin, A., Okou, R., Barendse, P., Khan, M. A., & Pillay, P. (2011). *Control of a flywheel energy storage system for rural applications using a Split-Pi DC-DC converter*. In 2011 IEEE International Electric Machines & Drives Conference (IEMDC), Niagara Falls, ON, Canada, pp. 265–270.

- Nakajima, T., & Irokawa, S. (1999). *A control system for HVDC transmission by voltage sourced converters*. In 199 IEEE Power Engineering Society Summer Meeting. Conference Proceedings (Cat. No.99CH36364), Edmonton, Alta., Canada, pp. 1113–1119.
- Natori, K., Obara, H., Yoshikawa, K., Hiu, B. C., & Sato, Y. (2014). *Flexible power flow control for next-generation multi-terminal DC power network*. In 2014 IEEE Energy Conversion Congress and Exposition (ECCE), Pittsburgh, PA, USA, pp. 778–784.
- Oday, A. (2011). *Investigation into high efficiency DC-DC converter topologies for a DC microgrid system*. Ph.D thesis, University of Leicester.
- Park, J., Kwon, M., & Choi, S. (2013). Design and Control of a Bi-directional Resonant DC-DC Converter for Automotive Engine/Battery Hybrid Power Generators 7.
- Phattanasak, M., Gavagsaz-Ghoachani, R., Martin, J.-P., Pierfederici, S., & Davat, B. (2011). *Flatness based control of an isolated three-port bidirectional DC-DC converter for a fuel cell hybrid source*. In 2011 IEEE Energy Conversion Congress and Exposition, Phoenix, AZ, USA, pp. 977–984.
- Rathore, A., Patil, D., & Srinivasan, D. (2016). Non-isolated bidirectional soft switching current fed LCL resonant DC/DC converter to Interface energy storage in DC microgrid. *IEEE Transactions on Industry Applications*, 52(2): 1–1.
- Rey-López, J. M., Vergara-Barrios, P. P., Osma-Pinto, G. A., & Ordóñez-Plata, G. (2015). Generalities about Design and Operation of Micro grids., *DYNA* 2015, 82(192), 109–119.
- Rycroft, M. (2014). The emerging 400 V DC microgrid, EE Publishers Home.
- Shenai, K., Jhunjhunwala, A., & Kaur, P. (2016). Electrifying India using solar DC microgrids. *IEEE Power Electronics Magazine*, 3, 42–48.
- Singhai, M., Pilli, N., & Singh, S. K. (2014). *Modeling and analysis of split-Pi converter using State space averaging technique*. In 2014 IEEE International Conference on Power Electronics, Drives and Energy Systems (PEDES), Mumbai, India, pp. 1–6.
- Yao, L., Cui, H., Zhuang, J., Li, G., Yang, B., & Wang, Z. (2016). *A DC power flow controller and its control strategy in the DC grid*. In 2016 IEEE 8th International Power Electronics and Motion Control Conference (IPEMC-ECCE Asia), Hefei, China, pp. 2609–2614.